Royal Military Academy

TN515 : Communication Subsystems

Project Antennas

Officer-Student Beerten Pieter
Officer-Student De Schampheleire Ben

Department CISS

Under supervision of :
Maj. Becquaert, Mathias
Mr. Bontemps, Luc

Brussels,
December 14, 2022

Contents

List of Figures

1 Introduction

The use of drones in certain military environments has become essential. In order to communicate with a drone, an antenna needs to be installed. Unfortunately, this antenna is often a weak point of the aerial vehicle. Therefore, it could be interesting to utilize the chassis of the drone as an antenna. To put this to test, two cylindrical monopole antennas were fabricated based on the carbon construction of a particular drone. This simulates the use of the carbon chassis as an antenna, but offers more flexibility and allows for easier testing.
In this report, a series of measurements is performed on these handmade monopole antennas. The report itself consists of two major parts. On the one hand, a characterization of the antennas will be performed. Concretely, the bandwidth and center frequency are determined, followed by the calculation of the three regions around the antennas. Next, one of the antennas will be adapted to match the impedance of the transmission lines. After this, the radiation pattern in both azimuth and elevation is determined. This first part is concluded with a determination of the gain of both antennas. The second part on the other hand treats the different propagation models. Calculations will be done for the free space link model, as well as for the Two-Ray model and the small-scale fading model.

2 Provided equipment

Before discussing the actual measurements performed in this report, the provided equipment will first be detailed.

2.1 Physical description of the antennas

As stated in the introductory paragraph, the considered antennas are cylindrical monopole antennas crafted with the chassis of a drone. In Figure 1, one of these antennas is shown.

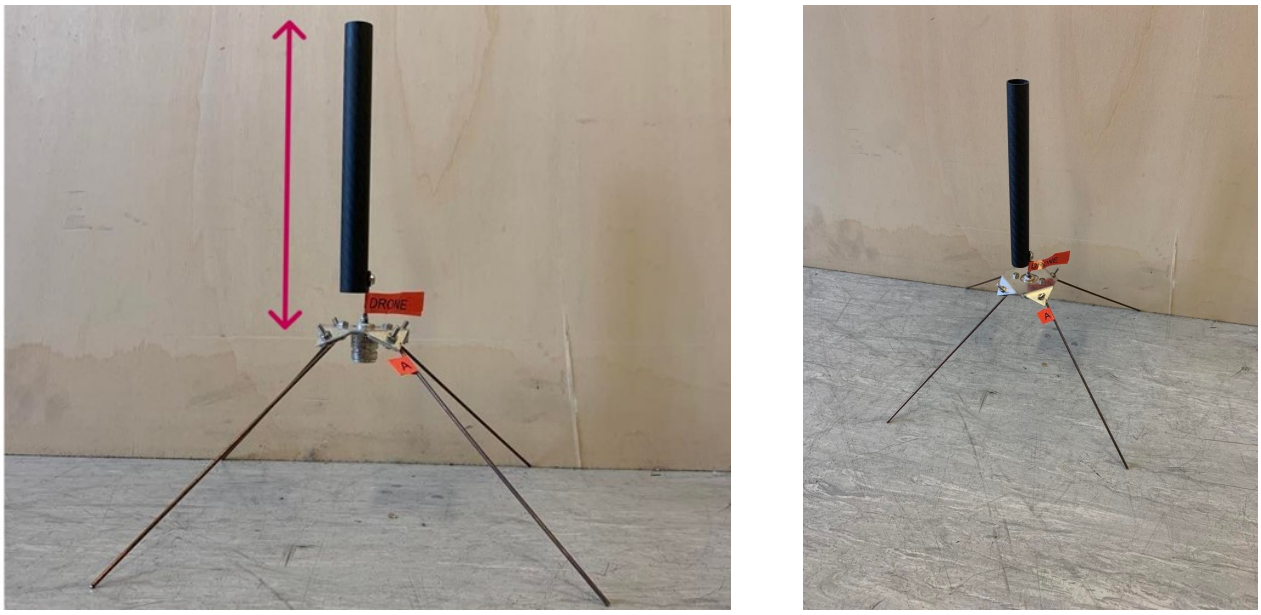

Figure 1: Drone antenna

In order to perform the necessary measurements on both of the antennas, one should know their dimensions, but most importantly the characteristic length. For a monopole antenna, this is nothing else than the maximal dimension of the antenna. Applied to the drone antennas used in this report, this corresponds to the length of the black tube and the small metal rod, stopping at the metallic ground plane, as shown with the red arrow on the left side of Figure 1. For both antennas, the characteristic dimension is 16.9 cm. Of course, this parameter does not suffice to completely characterize the antenna. Another important measure is the diameter of the cylindrical tube, equal to 1.5 cm. Also, the dimensions of the ground plane were measured, as well as the length of the legs of the antenna, the radials. The ground plane is 4.5 $cm \times 4.5$ cm and the radials measure 17.0 cm.

2.2 Vector Network Analyzer

A Vector Network Analyzer (VNA) can be used to measure the frequency response of components in a network. Here, it is used for the measurement of the reflection coefficient of both antennas.

Figure 2: Vector Network Analyzer

2.3 Signal generator

Throughout the different measurements, a signal generator of *Rohde & Schwarz* is used. This device allows to generate waveforms with a specific amplitude and frequency. Besides, it also allows to perform different types of modulations.

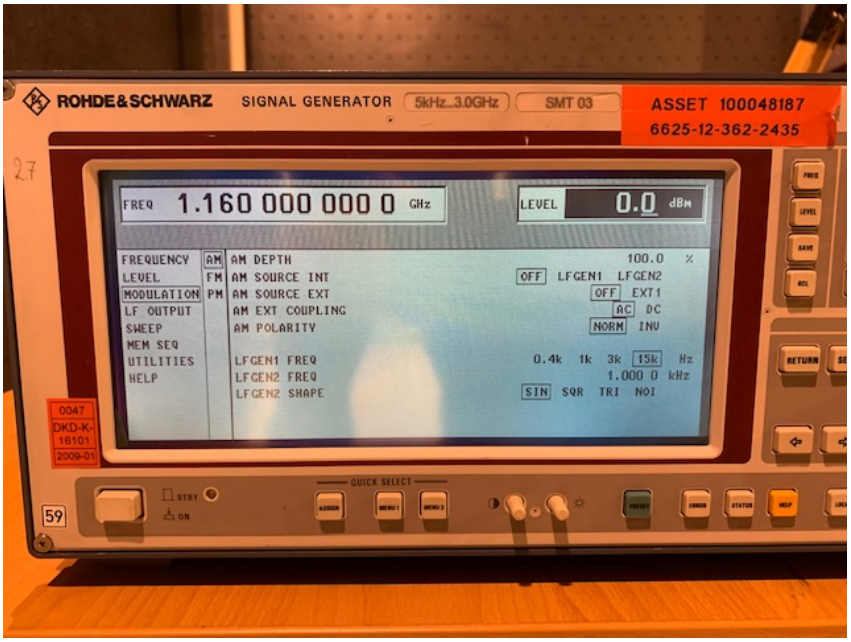

Figure 3: Signal generator

2.4 Spectrum analyzer

In order to determine how much power was received by a certain antenna, a spectrum analyzer is used. This devices allows to visualize the received power over a certain frequency range and is shown in the following Figure.

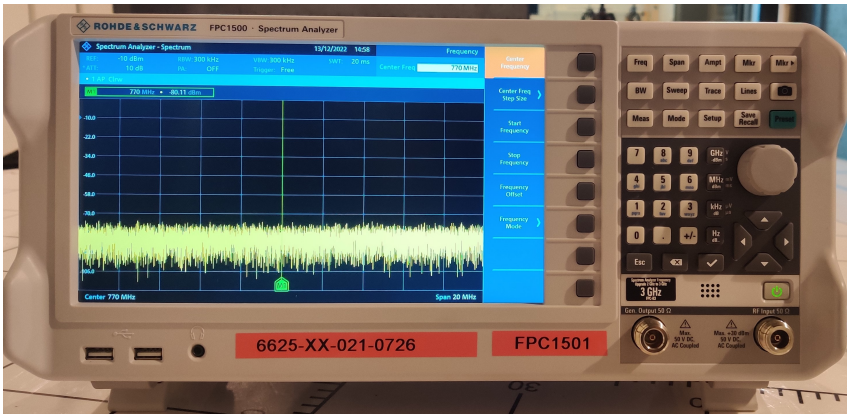

Figure 4: Spectrum analyzer

2.5 Electromagnetic field measurement device

At some point, the strength of the electrical field will have to be measured. The device used for this is called an *electromagnetic field measurement device* (EMD) and is represented in Figure 5.

Figure 5: Electromagnetic field measurement device

3 Characterization of the antennas

In this section, the characteristics of both antennas will be measured and discussed. First of all, the bandwidth is discussed. Therefore, the reflection coefficient is measured as well as the Voltage Standing Wave Ratio (VSWR). The measured VSWR will also be compared to its theoretical value. Based on the VSWR, the working bandwidth and center frequency are determined. Secondly, the boundaries of the different regions of the antenna are calculated. Thirdly, the impedance of the antenna is matched to the characteristic impedance of the transmission lines by considering only lossless lines. Finally, the radiation pattern in azimuth and elevation is measured and the gain of the antennas is determined.

3.1 Discussion on the bandwidth

3.1.1 Setup

Before beginning the discussion on the bandwidth, the used setup is first described. In order to perform the measurements in this chapter, the antenna was placed on a tripod and connected to the measurement device using a coaxial cable, as shown in following Figure.

Figure 6: Setup for the discussion of the bandwidth

No special attention was given to the surroundings of the antenna, since this has a minimal influence on the readings of the reflection coefficient and the VSWR. However, for the remainder of this report, the influence of the surroundings will play a role and will be taken into account.

3.1.2 Reflection coefficient

As a first step in the analysis of the performance of these antennas, the complex reflection coefficient s_{11} is determined using the Vector Network Analyzer (VNA). This parameter indicates to what extent an electromagnetic wave is reflected due to a discontinuity in the impedance of a medium. Solely the magnitude of this complex parameter is of importance for this report. Therefore, the phase will never be considered. Before the measurements can be done, the device needs to be calibrated of course. The calibration was performed by following the prescribed steps on the VNA and will not be detailed in this report. The resulting graphs for both antennas are given in Figure 7.

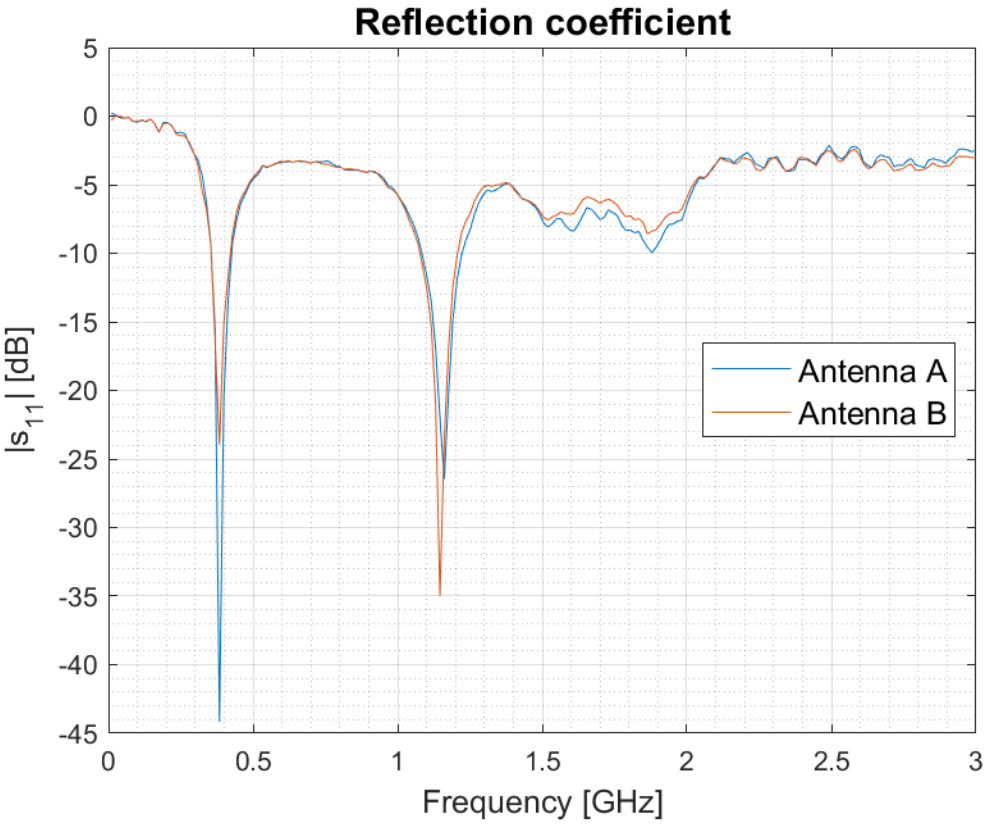

Figure 7: Magnitude of the reflection coefficient s_{11}

One can clearly notice the magnitude of the reflection coefficient shows two negative peaks, occurring at about the same frequencies for both antennas. These peaks indicate the frequencies where almost no reflections occur and thus the favorable domains of the antennas. These curves will later be used to deduce the VSWR.

3.1.3 Voltage Standing Wave Ratio

Next, the VSWR is measured for both antennas using the calibrated VNA. The VSWR can also be calculated according to the following formula:

$$\text{VSWR} = \frac{1 + |s_{11}|}{1 - |s_{11}|} \tag{1}$$

where $|s_{11}|$ is the magnitude of the measured reflection coefficient. The results for the measured and calculated VSWR are shown in Figures 8 and 9, respectively.

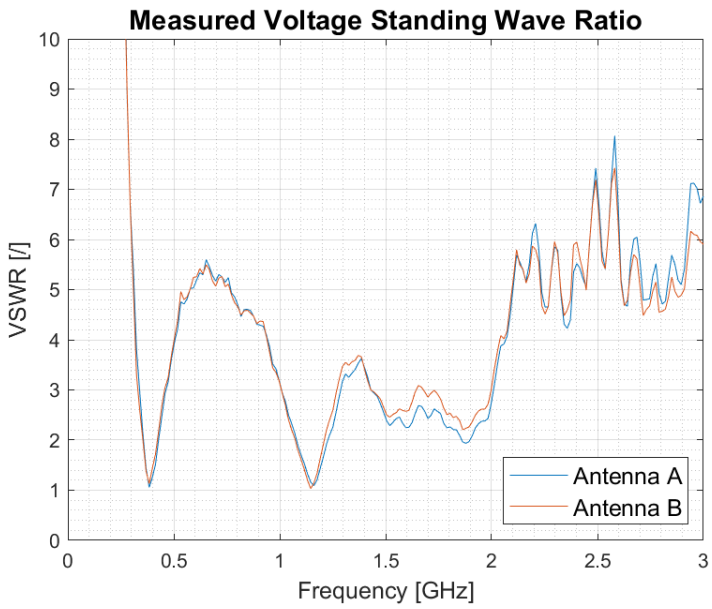

Figure 8: Measured VSWR

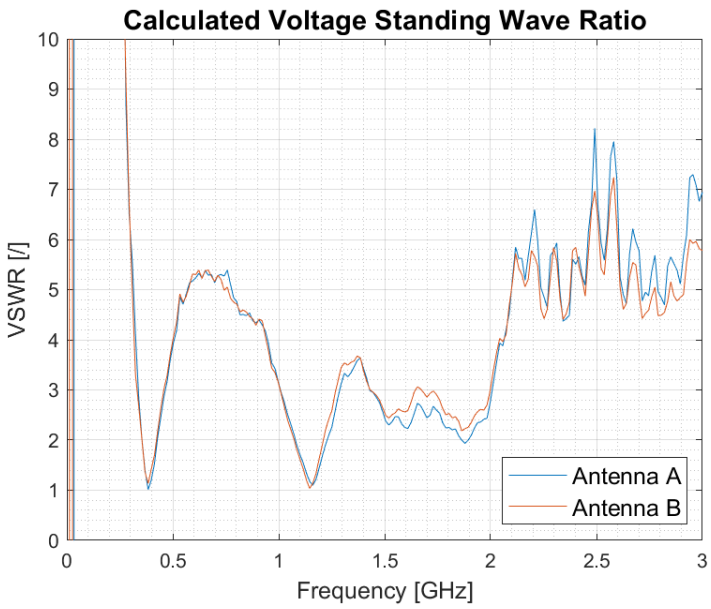

Figure 9: Calculated VSWR

One can easily notice similar results are obtained for both antennas using the two approaches. This already indicates an important similarity between the two antennas. Any difference that does exist is due to the fact that the antennas were handcrafted and thus not fabricated industrially, which would significantly reduce the error margins.
Finally, the measured and calculated VSWR are compared for each antenna individually. This allows to verify if the measurements are accurate with respect to the theoretical values. Therefore, both curves are superimposed for each antenna in Figure 10. This Figure shows that both methods indeed yield similar results.

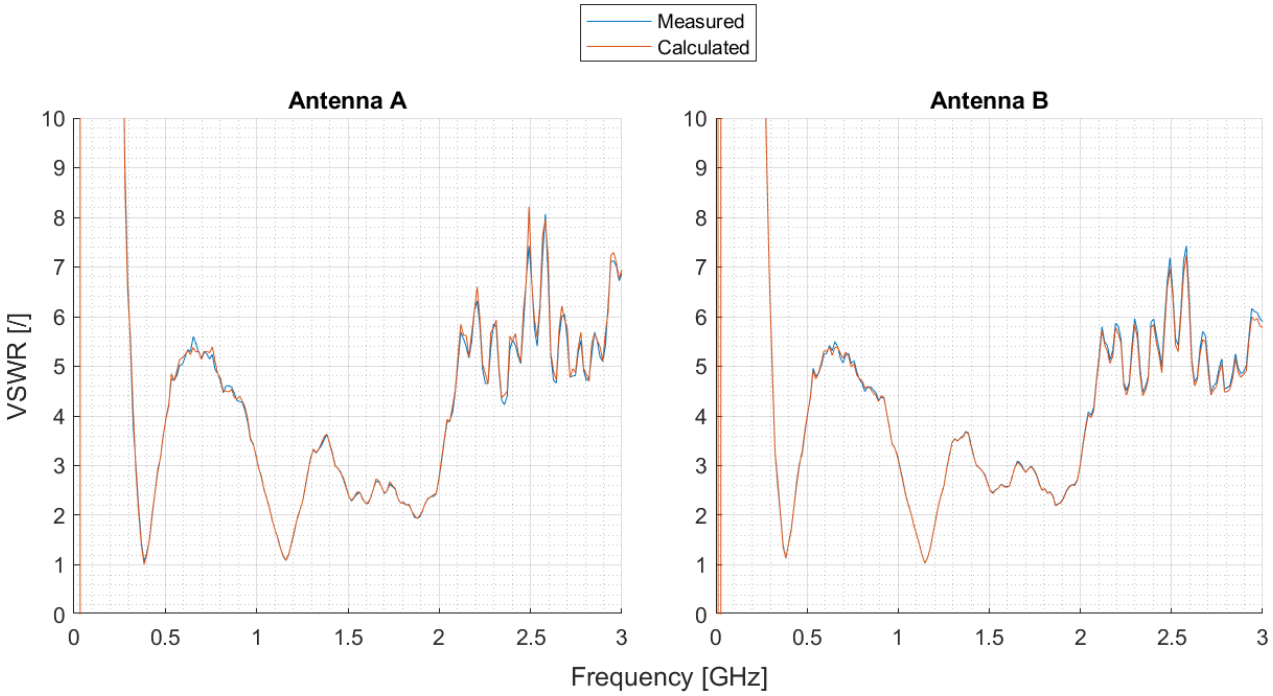

Figure 10: Comparison of the measured and calculated VSWR

3.1.4 Bandwidth and center frequency

Some of the most important properties to determine are the working bandwidth and center frequency of both antennas. The working bandwidth of an antenna can be defined as the frequency span in which the VSWR is below 2. In this region, at least 89% of the incoming power is transferred to the antenna for radiation. For both antennas, there are two regions that meet this requirement. They are indicated in Figure 11 below. Note that the measured VSWR is used for this approach. By looking at the Figure 10, one can clearly see that the two curves coincide for the regions of interest, meaning this choice will have no influence whatsoever.

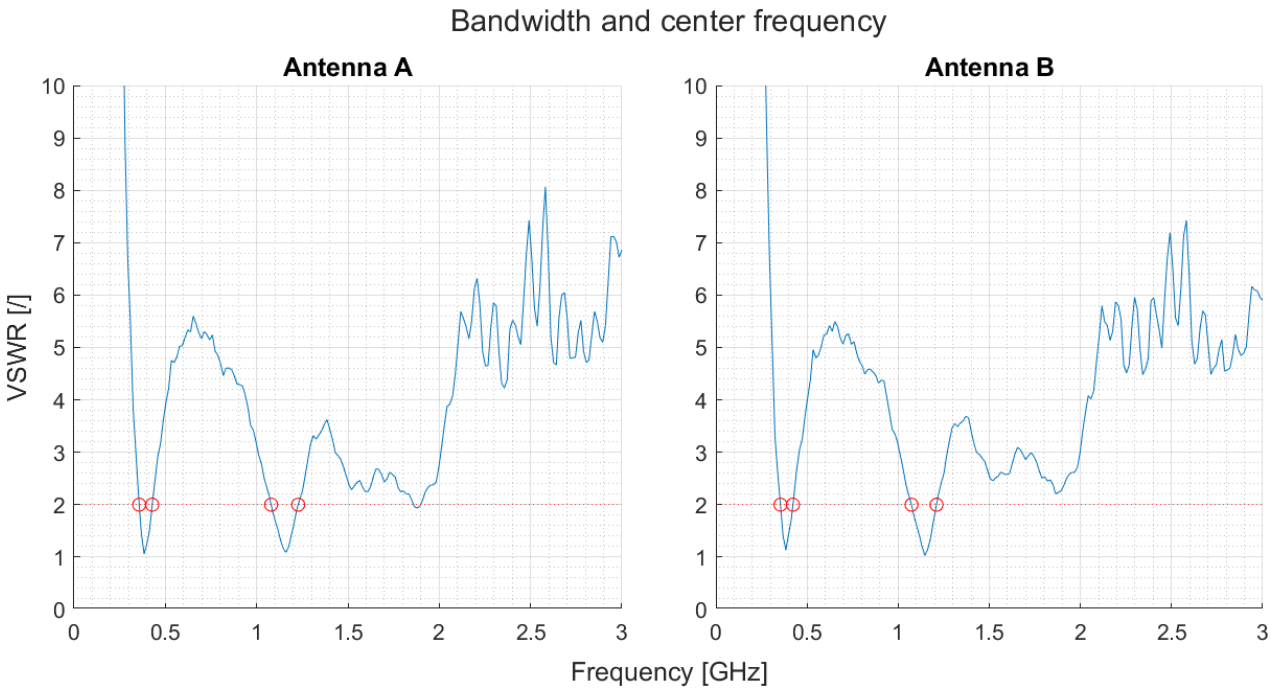

Figure 11: Bandwidth for both antennas

The center frequency corresponds to one of the two negative peaks located within the bandwidth. The choice will depend on the resulting available bandwidth for each of these frequencies. An overview of the center frequencies and corresponding bandwidths is given in the following Tables.

f_{center}	Bandwidth
383.75 MHz	71.23 MHz
1.16 GHz	148.12 MHz

Table 1: Antenna A

f_{center}	Bandwidth
383.75 MHz	68.50 MHz
1.15 GHz	137.00 MHz

Table 2: Antenna B

One can notice that the center frequency for the first region is equal for both antennas, while the center frequency of the second region shows a slight difference. From the previous Figure and Tables, it is clear that a center frequency of about 1.16 GHz yields the largest bandwidth for both antennas. However, since one frequency will be used for further experiments, a choice has to be made. In this case, the bandwidth corresponding to 1.16 GHz is larger than the bandwidth around 1.15 GHz. Therefore, the former is retained as the center frequency for both antennas.

3.1.5 Regions around the antennas

Now that the bandwidth and center frequency have been determined, it is possible to calculate the boundaries of the different regions around the antenna. The Reactive Near-Field is situated closest to the antenna. It is followed by respectively the Fresnel and Fraunhofer regions. In the latter, the electromagnetic waves can be considered as planar waves, simplifying a lot of the theoretical equations. A schematic overview is given in Figure 12.

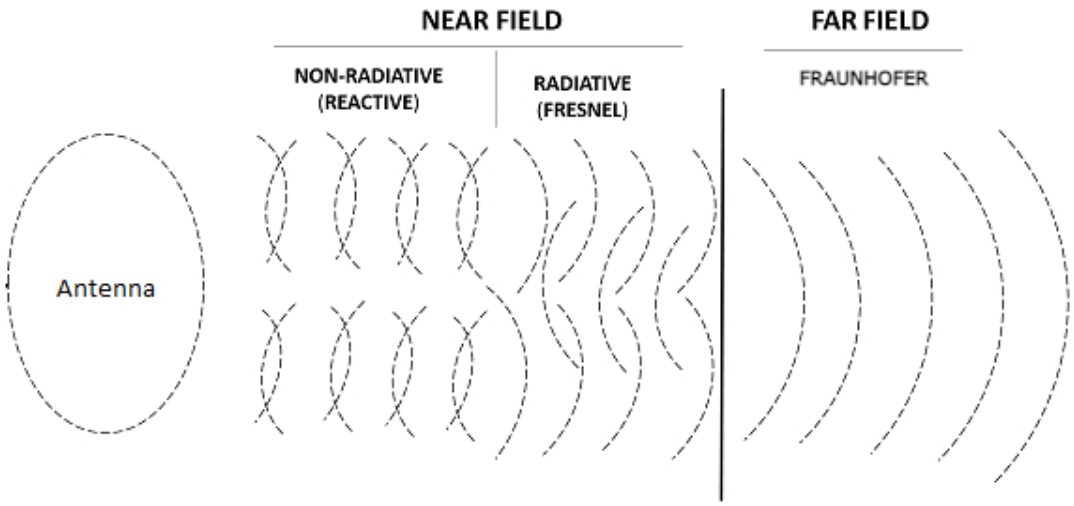

Figure 12: Overview of the regions around and antenna [6]

For the Fresnel region, this distance can be calculated using the following set of formulas:

$$\begin{cases} R > 20 \cdot \dfrac{\lambda}{2\pi} \\ R > 20 \cdot \rho_{max} \\ R \geq 0.6 \cdot \sqrt{\dfrac{D^3}{\lambda}} \end{cases} \tag{2}$$

The start of the Fraunhofer region can be calculated with a similar set of formulas:

$$\begin{cases} R > 20 \cdot \dfrac{\lambda}{2\pi} \\ R > 20 \cdot \rho_{max} \\ R > \dfrac{2D^2}{\lambda} \end{cases} \tag{3}$$

To determine at what distance these regions start, the least restrictive formula of the set is applied. Put differently, the boundaries correspond to the minimal distance R for which all three equations are respected. The results obtained by filling in these different formulas with the chosen center frequency ($1.16\ GHz$) and the measured characteristic dimension ($16.9\ cm$) are listed in the following Tables.

Formula	Distance [m]
$20 \cdot \frac{\lambda}{2\pi}$	0.822
$20 \cdot \rho_{max}$	3.380
$0.6 \cdot \sqrt{\frac{D^3}{\lambda}}$	0.082

Table 3: Boundaries for the Fresnel region

Formula	Distance [m]
$20 \cdot \frac{\lambda}{2\pi}$	0.822
$20 \cdot \rho_{max}$	3.380
$\frac{2D^2}{\lambda}$	0.221

Table 4: Boundaries for the Fraunhofer region

Utilizing this approach, the boundaries of the Fresnel and Fraunhofer regions will thus coincide for both antennas at a distance of 3.38 m from the antenna. Given the dimensions of the testing laboratory, measurements can always be performed in the Fraunhofer region.

3.2 Impedance matching

In this section, one of the antennas will be matched to the impedance of the transmission line in order to reduce reflections as much as possible. This way, the efficiency of the antenna can be optimized, which results in a maximal range and longest lifetime of the antenna. The process comes down to moving the operating point to the center of the Smith Chart, which corresponds to a pure resistance of 50 Ω [2]. Impedance matching can be achieved by adding either an open or a short-circuited parallel stub (i.e. a piece of cable considered lossless) to the circuitry, or by using lumped elements such as capacitors, inductors and resistors. For this report, the only available option is to add a parallel open or shorted stub.

In Figure 13, the Smith Chart of both antennas before impedance matching is shown. It can be verified that the working points of both antennas at the center frequency already lie very closely to the center.

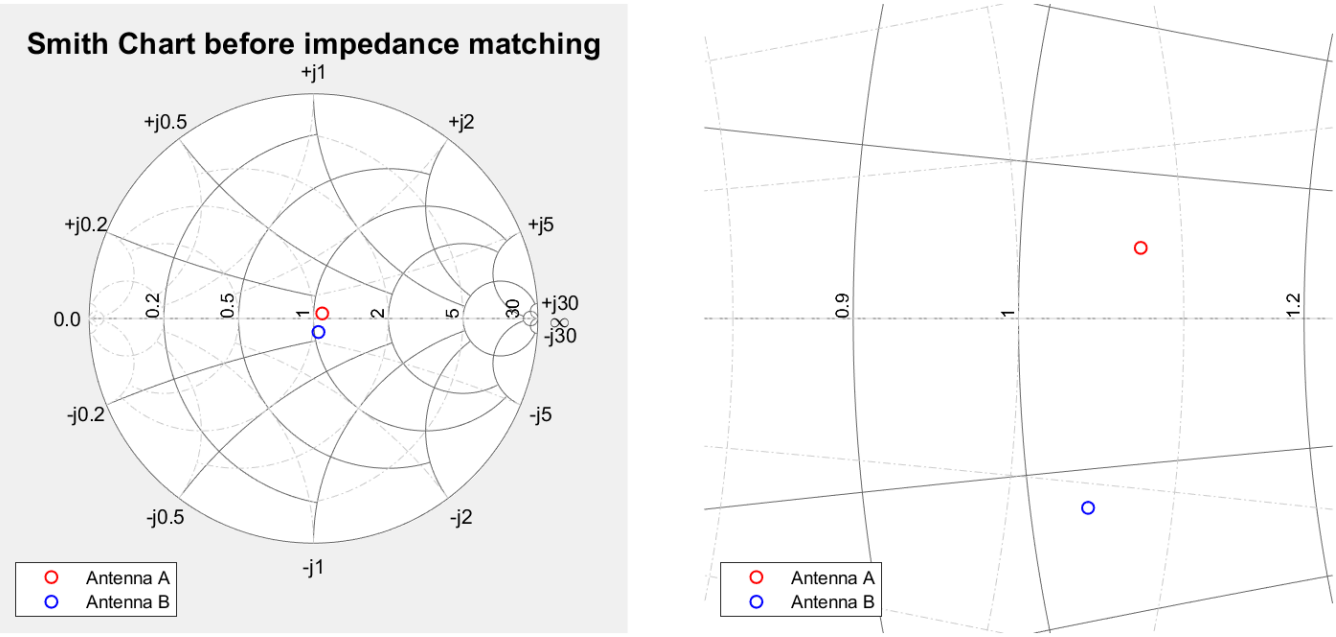

(a) Smith Chart

(b) Zoom of the Smith Chart

Figure 13: Smith Chart before impedance matching

In order to calculate the length and location of the stub, one needs to know the type of stub that is going to be used. For this report, *RG58 Coaxial cables* are available for use. These cables have a velocity factor of 66% [3], which should be taken into account. The calculation for antenna A will be detailed below. For antenna B, a similar calculation can be performed.

Adding a stub, be it an open or shorted variant, results in a combination of two effects. First, since the stub is placed at a certain distance from the load, it will initially have the same effect as adding a

lossless cable. Therefore, the addition of a stub will always result in a rotation around the center of the Smith Chart. Secondly, depending on the type, the addition of a stub will have another effect. When considering an open stub, the working point is displaced downwards on a circle of constant susceptance, similarly to the effect of a capacity. Conversely, the shorted stub displaces the working point upwards on a circle of constant susceptance, similarly to the effect of an inductor.

As a starting point for the calculation of the length and location of the stub, the following set of equations is used.

$$\begin{cases} |s_{11}| & = \left|\frac{1-y}{1+y}\right| = 0.0449 \\ \Re(y) & = 1 \end{cases} \tag{4}$$

The first equation corresponds to the definition of the reflection coefficient. Since the magnitude of this reflection coefficient is known for both working points, this equation corresponds to a circle around the center of the Smith Chart with radius $|s_{11}|$. The second equation represents the collection of working points that lie on a circle where the susceptance equals 1. These working points allow to easily go to the center of the Smith Chart by adding a parallel stub, since this will move the working point on a circle with constant susceptance.
The equations can then be combined.

$$|s_{11}| = \left|\frac{1-y}{1+y}\right| = \left|\frac{1-(1+b\cdot j)}{1+(1-b\cdot j)}\right| = \left|\frac{b^2-2b\cdot j}{b^2+4}\right| = 0.0449 \tag{5}$$

Solving this equation for b yields an infinity of solutions, each separated by a multiple of half the wavelength. Since every solution leads to the same end result but solely the first two solutions do so by using the least amount of cable, only these solutions are kept. They correspond to $b = \pm 0.09$, or $y_1 = 1 + 0.09\,j$ and $y_2 = 1 - 0.09\,j$.
From these values of y_1 and y_2, the corresponding reflection coefficients can be calculated:

$$\begin{cases} K_1 & = \dfrac{1-y_1}{1+y_1} = -0.002 + 0.0449\,j \\ K_2 & = \dfrac{1-y_2}{1+y_2} = -0.002 - 0.0449\,j \end{cases} \tag{6}$$

For efficiency reasons, only the short-circuited stub, starting from y_2, will be considered as the open stub needs to be placed further from the load, resulting in more cable to be used.
First, the distance u from the load where the shorted parallel stub has to be added will be calculated. To this end, the following formula can be used.

$$j\,\tan\left(\frac{2\pi}{\lambda_{eff}}\cdot u\right) = \frac{Z_0\cdot(Z-Z_L)}{Z_0^2 - ZZ_L} \tag{7}$$

where λ_{eff} is the effective wavelength, calculated by multiplying λ with the velocity factor discussed above. Z_0 corresponds to the characteristic impedance, Z_L corresponds to the impedance of the load

and Z is the impedance corresponding to y_2.

From equation 7, one finds that $u = 2.90\ cm$.
To calculate the required length of the short-circuited stub, the circle of constant susceptance $\Re(y) = 1$ is followed until the center of the Smith Chart is reached. To reach the center from y_2, one should add a susceptance $-0.09\,j$. The calculation is given below.

$$\begin{cases} K &= \dfrac{1 - 0.09 \cdot j}{1 + 0.09 \cdot j} = 0.984 - 0.179 \cdot j \\ &= |1| < -0.1794 \\ l &= \dfrac{\lambda_{eff}}{4\pi} \cdot abs(-0.1794) = 0.24\ cm \end{cases} \tag{8}$$

In conclusion, to perform impedance matching for antenna A, one should at a short-circuited stub of length 0.24 cm at a distance of 2.90 cm from the load. For antenna B, a short-circuited stub of length 0.35 cm at a distance of 0.57 cm from the load should be added. In Figure 14, the impedance matching procedure is visualized for both antennas.

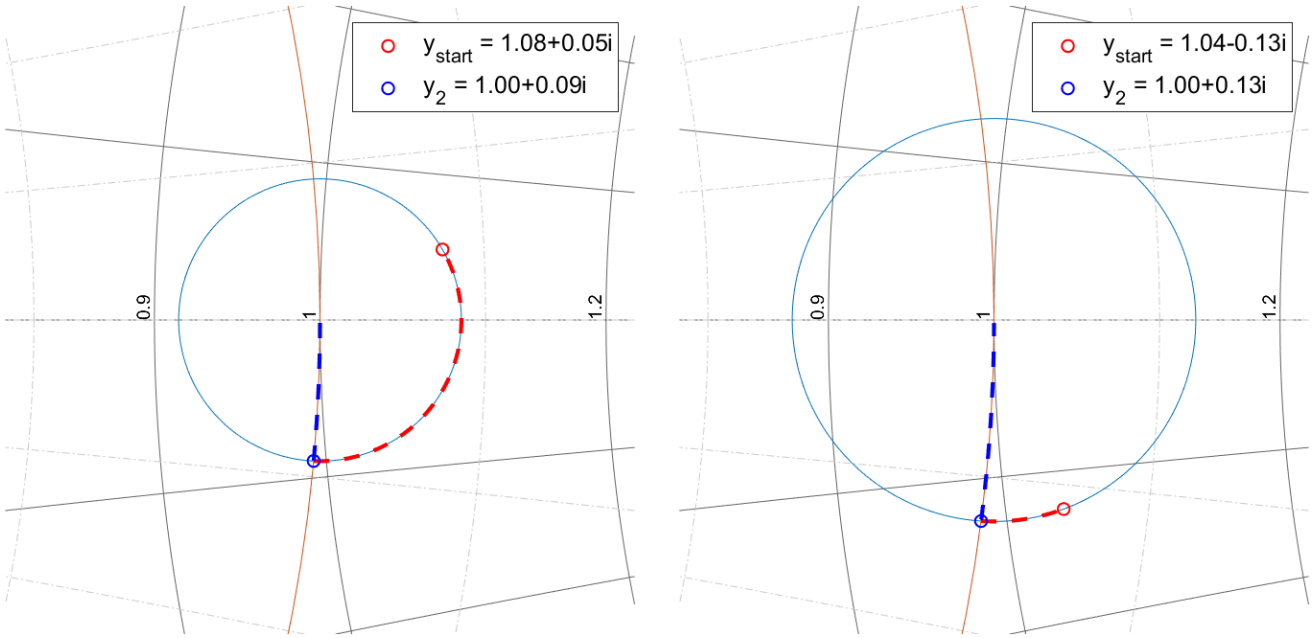

(a) Antenna A (b) Antenna B

Figure 14: Impedance matching

As manufacturing a stub smaller than 1 cm is practically unfeasible, both antennas will not be matched.

3.3 Radiation pattern

The next step in the characterization of the antennas is a discussion about the radiation pattern, both in azimuth and in elevation.

3.3.1 Setup

First, the setup will be described in detail. In order to evaluate the radiation pattern of both antennas, we need of course a transmitting antenna connected to a signal generator. In this case, we used a rectangular horn antenna installed on a tripod, which is shown in the following Figure. In section 2, the signal generator was already briefly discussed.

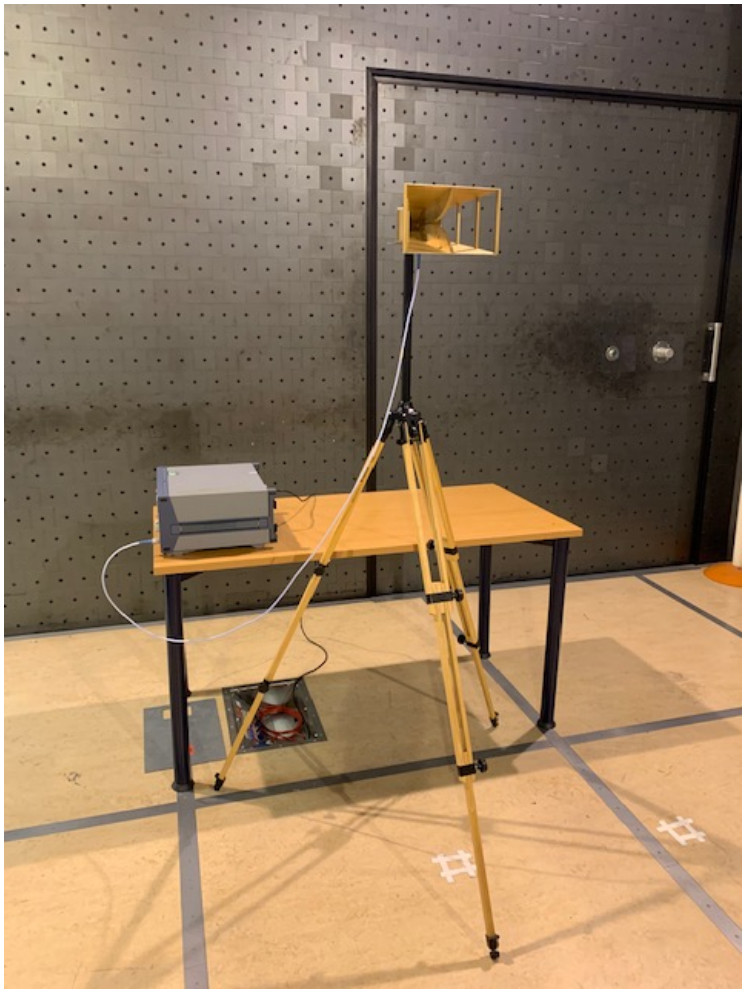

Figure 15: Horn antenna

In the Figure 3, one can also see the parameters used for these experiments. The horn antenna will transmit a signal at 1.16 GHz, corresponding to the center frequency previously determined, at 0 dBm. This power level should largely suffice for measurements on such a small scale.

On the receiver side, the drone antenna was placed on a similar tripod at the same height. However, the tripod was equipped with a fixation similar to a knee joint in order to allow movement of the antenna in all directions. This allows to measure different configurations under different angles without having to move the tripod, taking away a possible source of error. Moreover, the antenna was connected to a spectrum analyzer via the same type of coaxial cable, as shown in the next Figures. In section 2, the spectrum analyzer was already briefly discussed.

Figure 16: Receiving antenna

Figure 17: Spectrum analyzer

As can be seen in Figure 16, the coaxial cable used in this setup has a tendency to wind itself around the tripod. This introduces extra distortions in the measurement chain and could have a significant impact on the results. Since the spectrum analyzer is placed next to the receiving antenna, the presence of the person reading and logging the data will influence the measurements as well. However, because this presence is constant during the entire measurement campaign, this factor will be neglected in this setup.

3.3.2 Radiation pattern in azimuth

First of all, the radiation pattern in the azimuth direction is measured. This is done by keeping the antenna vertical and rotating it over a full 360° while measuring the received power every 5°. The resulting radiation pattern is shown in Figure 18.

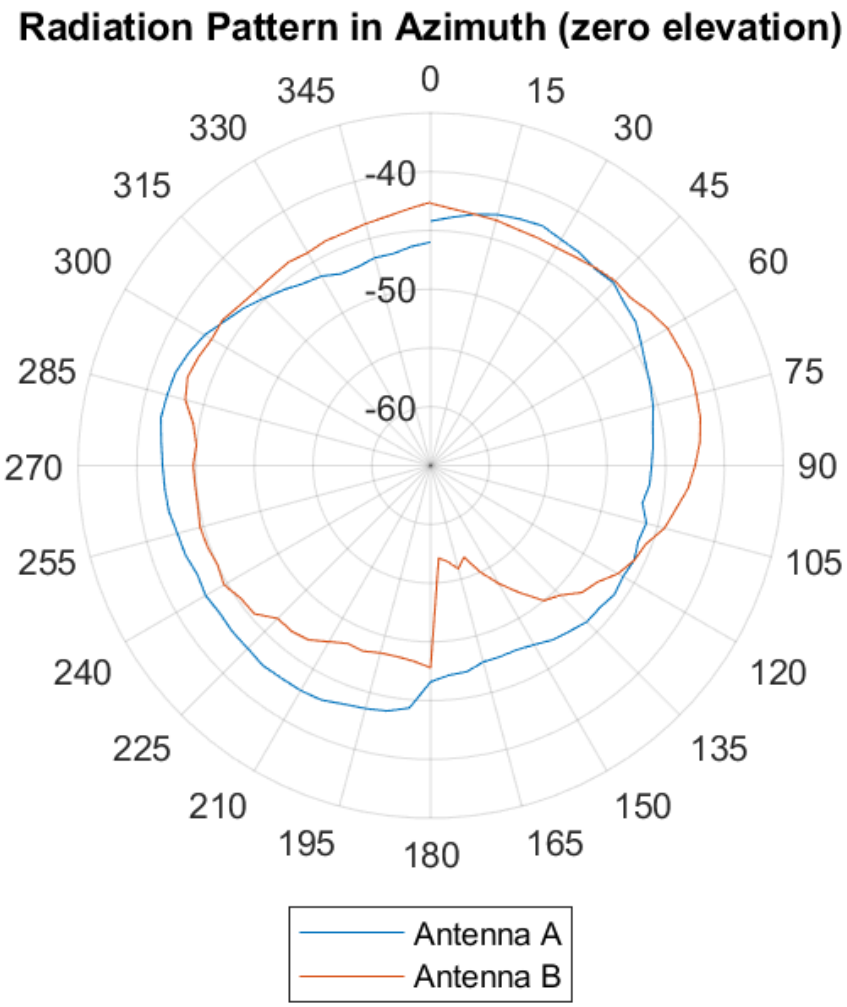

Figure 18: Radiation pattern in Azimuth

One immediately notices the enormous decline in power when antenna B approaches the 180° limit. This is caused by the cable that connects the antenna to the spectrum analyzer. For antenna B, this cable got twisted and stuck around the tripod onto which it was mounted, leading to a lot of losses in said cable. At 180°, the cable was disconnected and reconnected from the other side, removing the twist and leading to an apparent sudden increase in power. Independently of this observation, one can notice the overall form of the radiation pattern. The received power remains relatively constant over the entire azimuth. There are of course certain fluctuations, but these are mostly due to the movement of the cable after rotation. However, the form comes as no surprise since a theoretical monopole antenna has a circular radiation pattern in azimuth.

3.3.3 Radiation pattern in elevation

Secondly, the radiation pattern in elevation will be considered. Now, the measuring domain is limited to 180°, from $-90°$ (Rx antenna pointing towards the transmitter) to 90° (Rx pointing away from the transmitter). Measurements are still taken every 5°. The resulting radiation pattern is given in Figure 19.

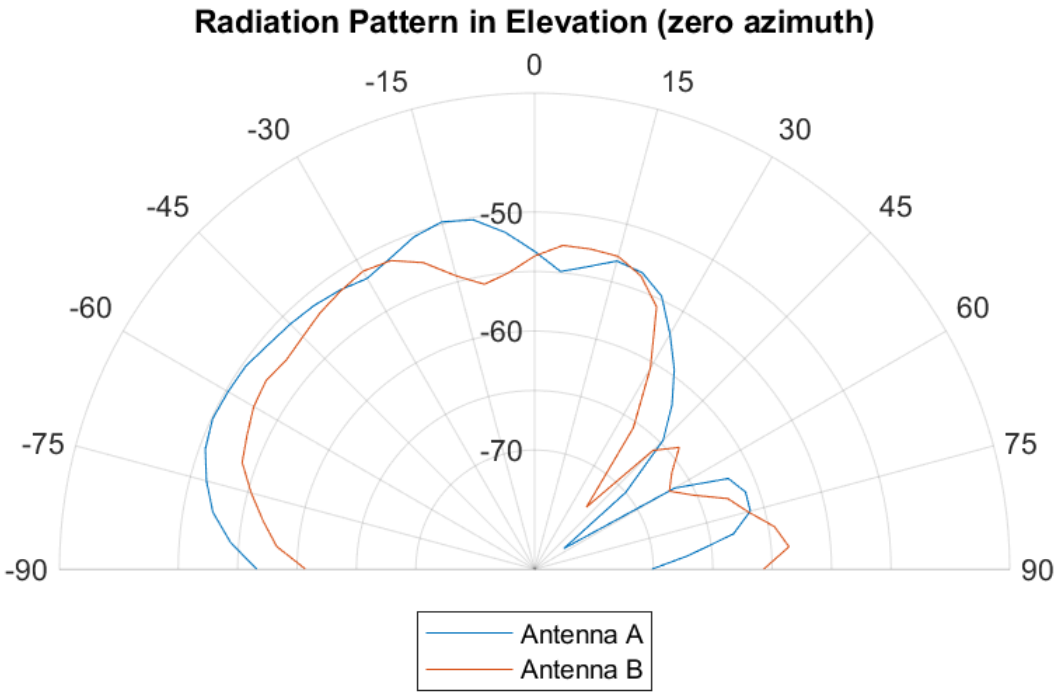

Figure 19: Radiation pattern in elevation

One can observe some strange behavior from 45° on. For these values of elevation, the monopole antenna is inclined such that the ground plane stands in line of sight with the transmitting antenna, leading to an apparent loss in received power. When the antenna is elevated in the other direction (i.e. for negative values of elevation), this phenomenon does not occur, since the antenna points directly towards the transmitting antenna.

In order to compare to the theoretical results, the drone antenna was simulated in Matlab using the *monopoleRadial* function and specifying the parameters. The material can also be specified but Matlab only accepts metals, so a carbon structure cannot be modelled. This will influence the results of the simulation. However, all the dimensions of the antenna can be correctly entered. A visualisation of the antenna's model is represented in Figure 20 below.

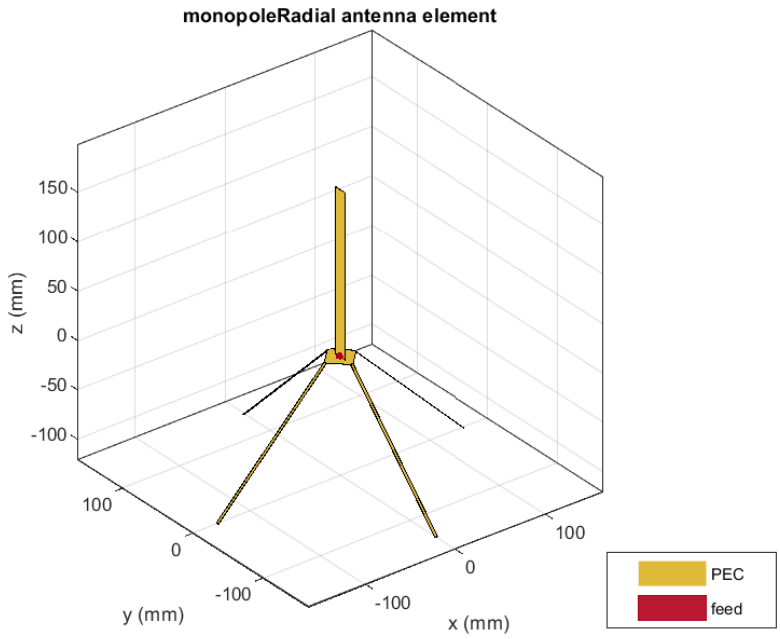

Figure 20: Model of the drone antenna

Using this model, the radiation pattern in elevation is represented at 1.16 GHz.

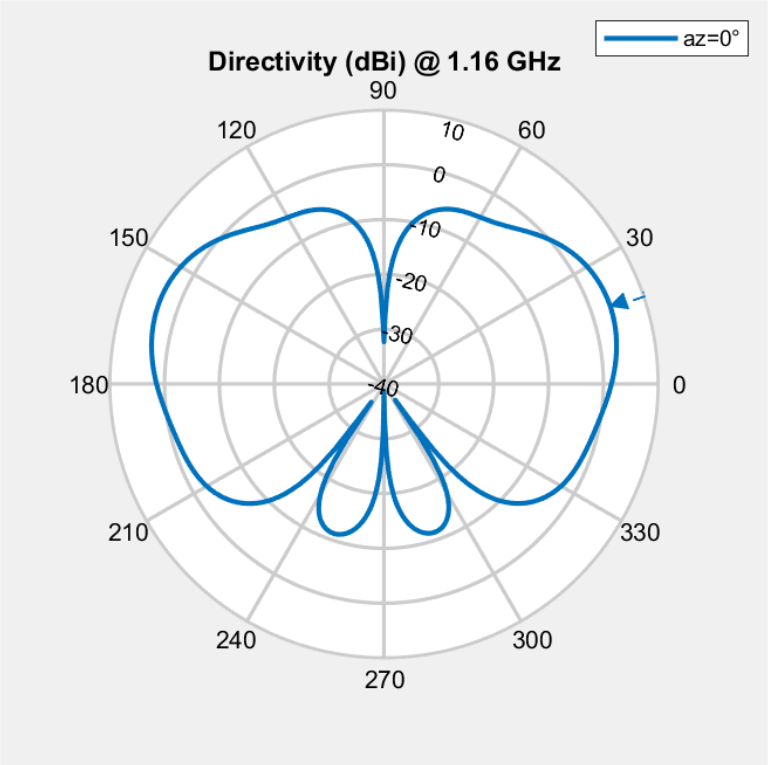

Figure 21: Simulated radiation pattern in elevation

Even though the used material is not correct, one can notice the general shape of the pattern between 90° and −90° (written here as 270°) is very similar to to shape of the measured pattern. However, the direction is inverted. This is because we chose a convention for the angle of elevation that is opposed to the convention used by Matlab. In any case, the large lobe between 90° and approximately −60° (300°) as well as the smaller side lobe between −60° (300°) and −90° (270°) correspond to the shape in Figure 19.

3.4 Determination of the gain

3.4.1 Setup

Before calculating the actual value of the gain, the test setup is first described. For the measurement of the gain, the same configuration is used as the previous section 3.3.1. Note however that the level of the transmitted power was now set to 10 dBm. Also, some anechoic blocks (radiation absorbers) were placed between the two antennas to limit ground reflections as much as possible. Additionally, the EMD, specified in section 2, was used to measure the electrical field strength.

3.4.2 Calculation of the gain

As a final part of the characterization of the antennas, the antenna gain is determined. For a transmitting antenna, the gain is an indication for how well the input power is converted into electromagnetic waves headed in a specified direction. For a receiving antenna, the gain indicates how well the antenna converts electromagnetic waves coming from a specified direction into electrical power [4].

To find the antenna gain, the following equation will be solved for G_r:

$$E = \sqrt{10^{\frac{P_{SA}}{10}} \cdot 10^{-3} \cdot \frac{480\pi}{\lambda^2} \cdot \frac{1}{10^{\frac{G_r}{10}}} \cdot \frac{1}{10^{\frac{att}{10}}}} \tag{9}$$

with:

1. E: the intensity of the electric field at the position of the antenna $\left[\frac{V}{m}\right]$
2. P_{SA}: the received power, measured with the spectrum analyzer [dBm]
3. G_r: the gain of the receiving antenna [dBi]
4. att: the attenuation of the cable [dB]

Note that in this equation, the receiving antenna gain is expressed in dBi. The i refers to isotropic, meaning the gain of the antenna is compared to its ideal, theoretical isotropic counterpart.

The intensity of the electric field E has to be measured at the exact same position as the receiving antenna, since it serves as a reference in the calculation using equation (9).

By using equation (9), a gain of -11.64 dBi is obtained for antenna A, and a gain of -9.74 dBi for antenna B. These negative gains indicate that the antennas actually perform worse than the isotropic reference antenna. Often, this is the result of internal losses or antenna mismatch. Also, one needs to consider that these antennas were handcrafted for testing purposes to simulate the chassis of a drone.

Since the antennas were not fabricated on an industrial scale, where the design is studied in detail and optimized, it is highly possible they are far from efficient.

4 Propagation models

Now that both antennas have been characterized, the different propagation models will be discussed. First of all, the free space link model model is analyzed. Secondly, the two-ray model is validated. Finally, the characteristics of a small-scale flat fading channel are determined.

Note that the transmitting horn antenna, used to characterize the two antennas, has now been replaced by antenna B. The resulting setup is shown below.

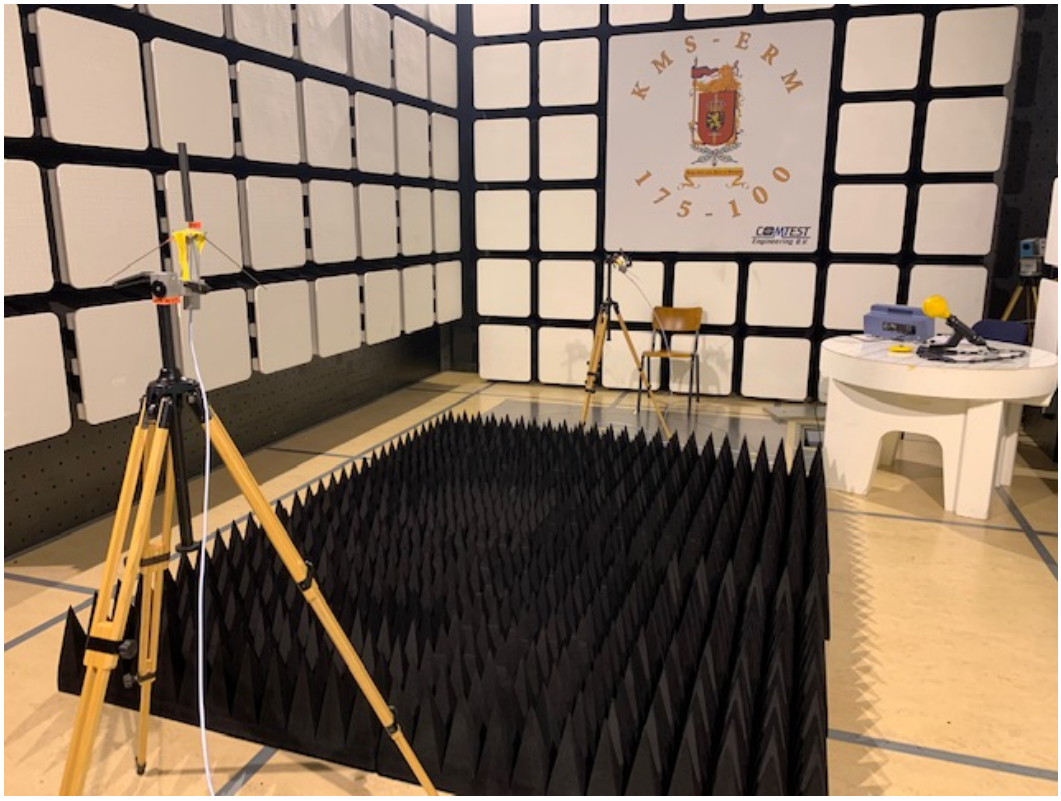

Figure 22: Setup for the propagation models

4.1 Free space link model

4.1.1 Received power as a function of distance

First of all, the received power is measured for different distances. To do this, a signal is transmitted at 1.16 GHz with a power of 10 dBm. In the Fraunhofer region, one would expect the power to be inversely proportional to the square of the distance, as predicted by the Friis equation.

$$P_{Rx} = \frac{P_{Tx}\, G_{Tx}\, G_{Rx}\, \lambda^2}{(4\pi R)^2} \tag{10}$$

The elements of this equation will not be elaborated and are considered known to the reader. The results of the measurements are shown in Figure 23.

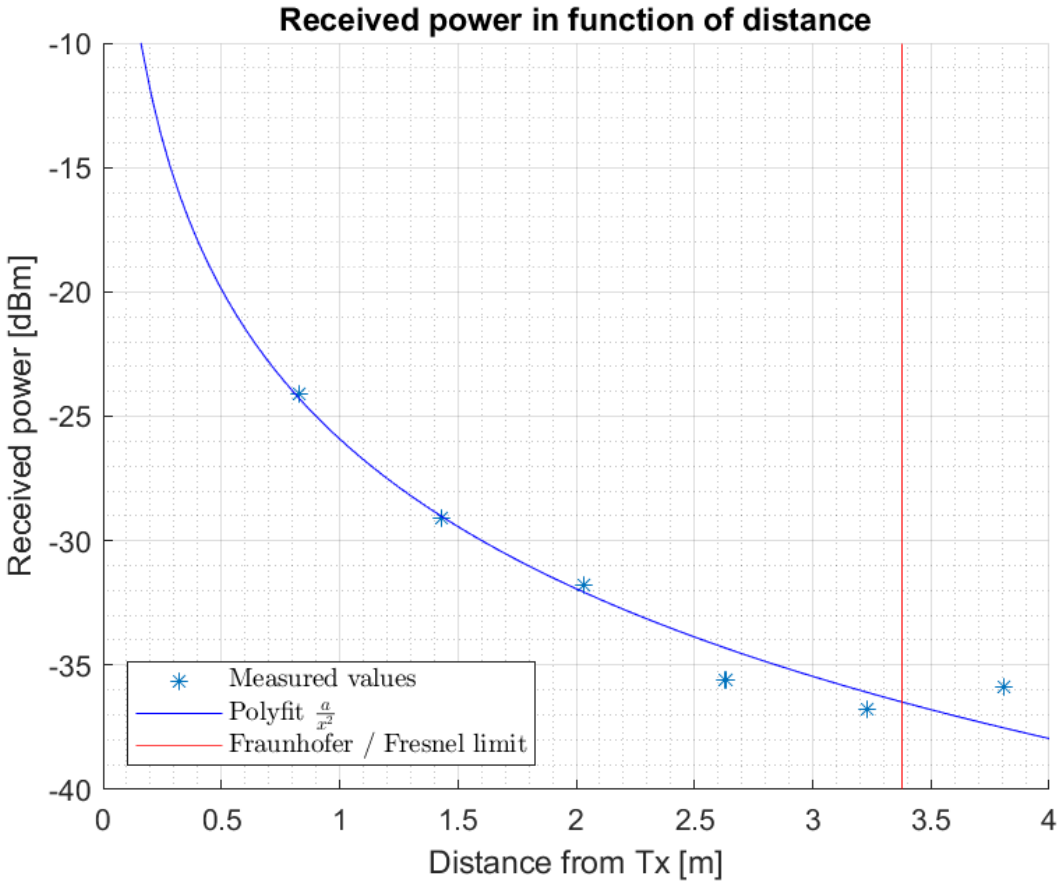

Figure 23: Received power for different distances

The polynomial fit of the second order indeed shows that the power is related to the distance from the transmitting antenna according to an inverse square law. However, the fit is not perfect. This is due to the fact that almost all measurements were taken in the reactive near field (due to limitations in dimensions of the laboratory), where the Friis equation is no longer valid.

4.1.2 Influence of a polarization mismatch

Secondly, the influence of a polarization mismatch on the received power is discussed. This can be measured by changing the orientation of the receiving antenna over an interval of 90° in the vertical plane. An angle of 0° corresponds to a perfect alignment of the two antennas.
The received power as a function of the polarization mismatch angle θ is plotted below in Figure 24.

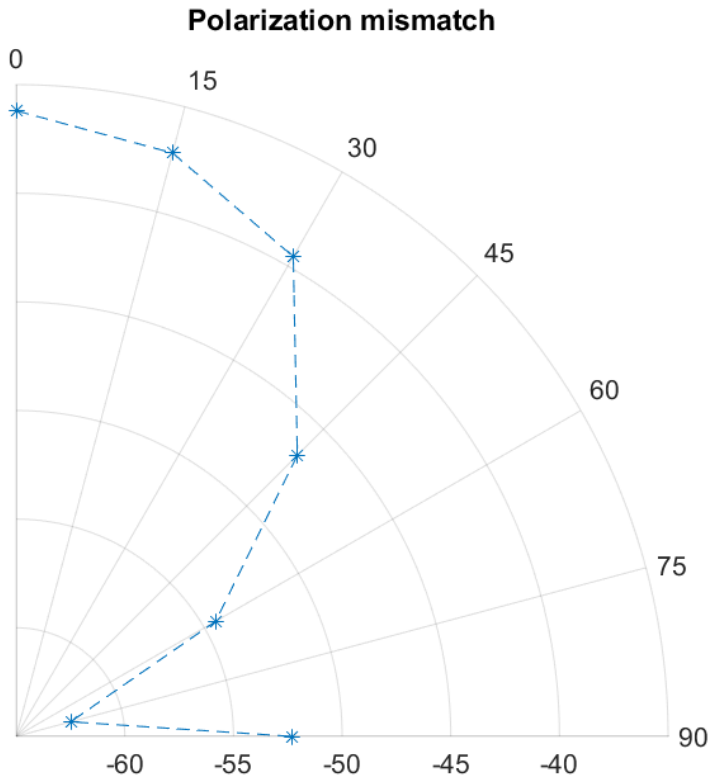

Figure 24: Received power for different polarization mismatch angles

From the above Figure it can be seen that the received power is highest for a mismatch angle of 0°. For higher angles, the received power diminishes. This is of course due to the increasing mismatch in polarisation. However, at an angle of 90°, the received power is significantly higher then before. One would actually expect it to disappear in the noise, since the electrical fields are perpendicular in this case. A clear explanation of this anomaly is yet to be found.

4.1.3 Influence of a relative angle between the antennas

Finally, the influence of a relative angle between the transmitting and receiving antenna is considered. To obtain these values, the receiving antenna was tilted over an interval of 180°, from $-90°$ to $+90°$ in steps of 15°. At an angle of $+90°$, the receiving antenna is pointing away from the transmitting antenna. At an angle of 0°, both antennas are aligned and at an angle of $-90°$, the receiving antenna is pointing towards the transmitter.

The resulting plot of the received power is given in Figure 25.

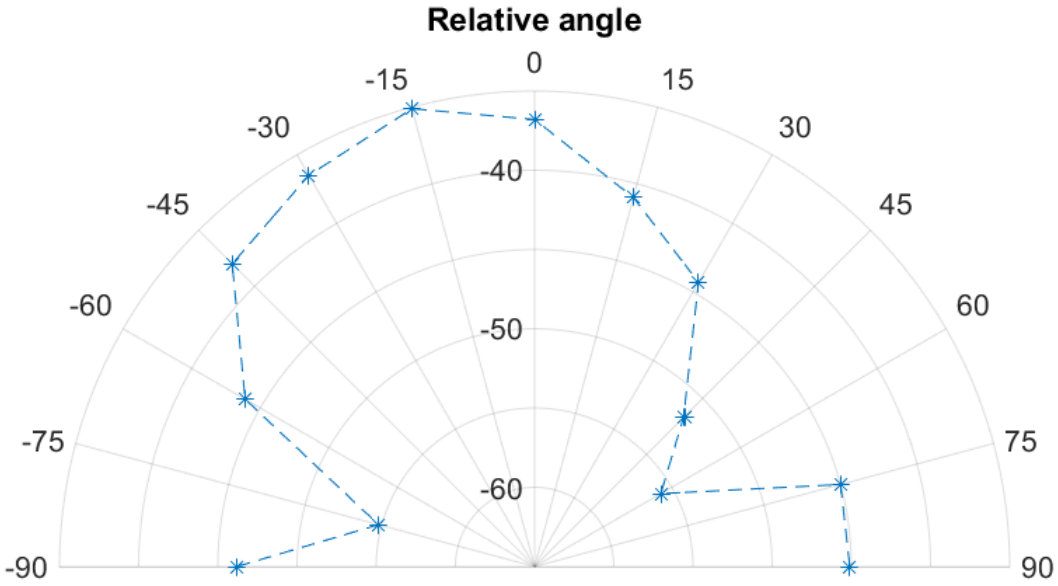

Figure 25: Received power for different relative angles

The chain of measurements performed here is actually very similar to the measurement of the radiation pattern in elevation. The only difference lies in the choice of the transmitting antenna; a horn antenna for the radiation pattern and the second drone antenna for this application. The received power appears to be maximal when the receiving antenna points toward the transmitting antenna under an angle of $-15°$. Moreover, a peculiar behavior is once again seen at the angles between $75°$ and $90°$, corresponding to the small side lobe.

4.2 Two-ray model

4.2.1 Explanation of the concept

The Two-Ray model is a multipath propagation model which predicts the path losses between two antennas that have a direct line of sight (LOS) between them. For this model, the received signal consist of a LOS component and a reflection coefficient, formed mainly by a single ground reflected wave [7].

An illustration of the concept is given in Figure 26 below.

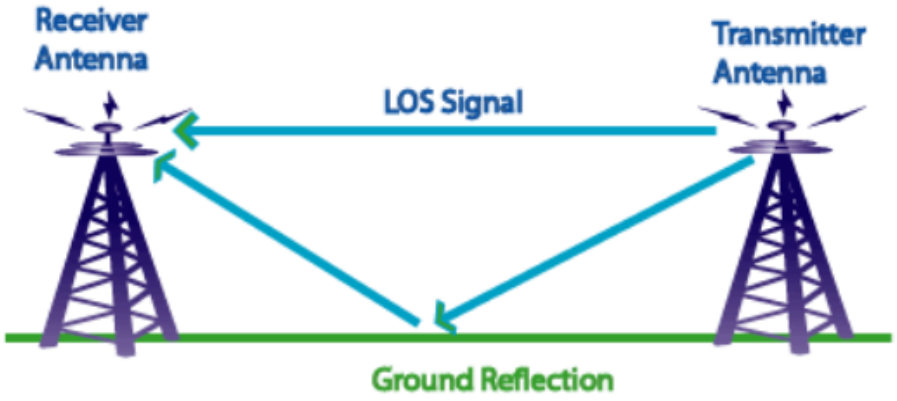

Figure 26: Illustration of the Two-Ray model [8]

4.2.2 Setup

To validate the Two-Ray model, the received power is measured for different setups. As a starting point, the entire distance between the transmitting and the receiving antenna is covered with radiation absorbers (consisting of anechoic tiles), for a total of five rows. In the different setups, the location and size of so-called *holes* (tiles without a radiation absorber) is varied. These holes will allow radiation to be reflected on the ground towards the receiving antenna, which could interfere with the direct radiation under particular circumstances. The antennas are placed at the same height to eliminate the influence of a difference in height. An example of a setup with one hole of unitary size at a position $Tx + 1$ is shown in Figure 27.

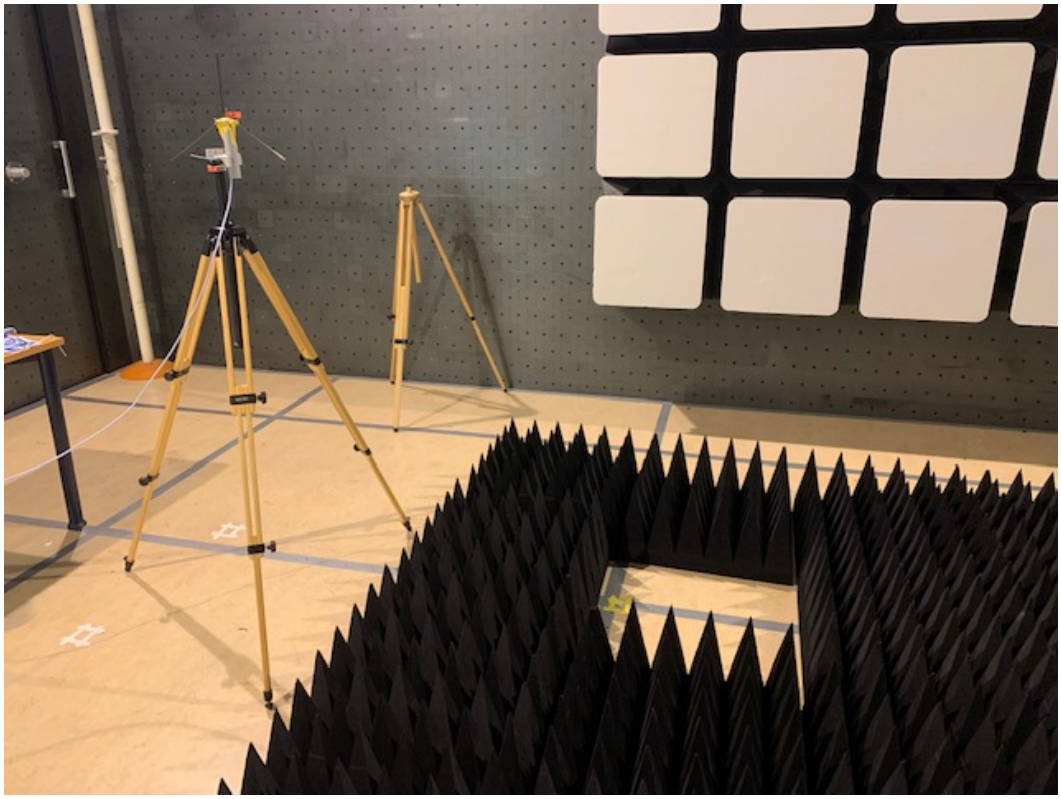

Figure 27: Setup for the validation of the two-ray model

4.2.3 Influence of the position of a hole

Before continuing with multiple holes, it is interesting to evaluate the influence of the position of the hole on the received power. Therefore, the received peak power is measured for every possible position of the hole, ranging from the Tx side all the way to the side of the receiving antenna. Since there are five rows of anechoic tiles, six possible configurations are put to test; the configuration with no holes is also considered. The results are shown in Figure 28.

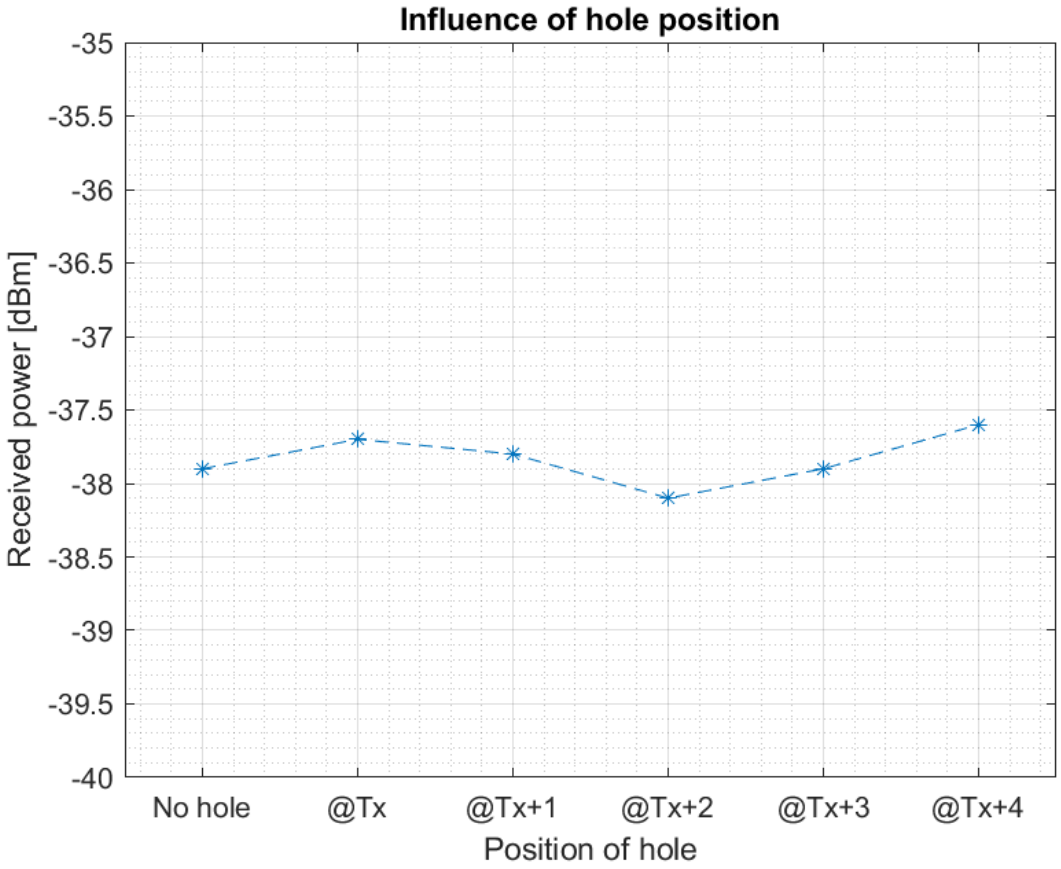

Figure 28: Influence of the position of a hole

It is clear that the variation between the measurements remains small. Indeed, the relative difference between the highest and lowest received power is only 1.33%. One can thus not conclude from these measurements that the position of hole has a significant influence on the received power.

4.2.4 Influence of the number of holes

Next, the number of holes in the setup is varied and the influence on the received power is measured. The results are shown in Figure 29.

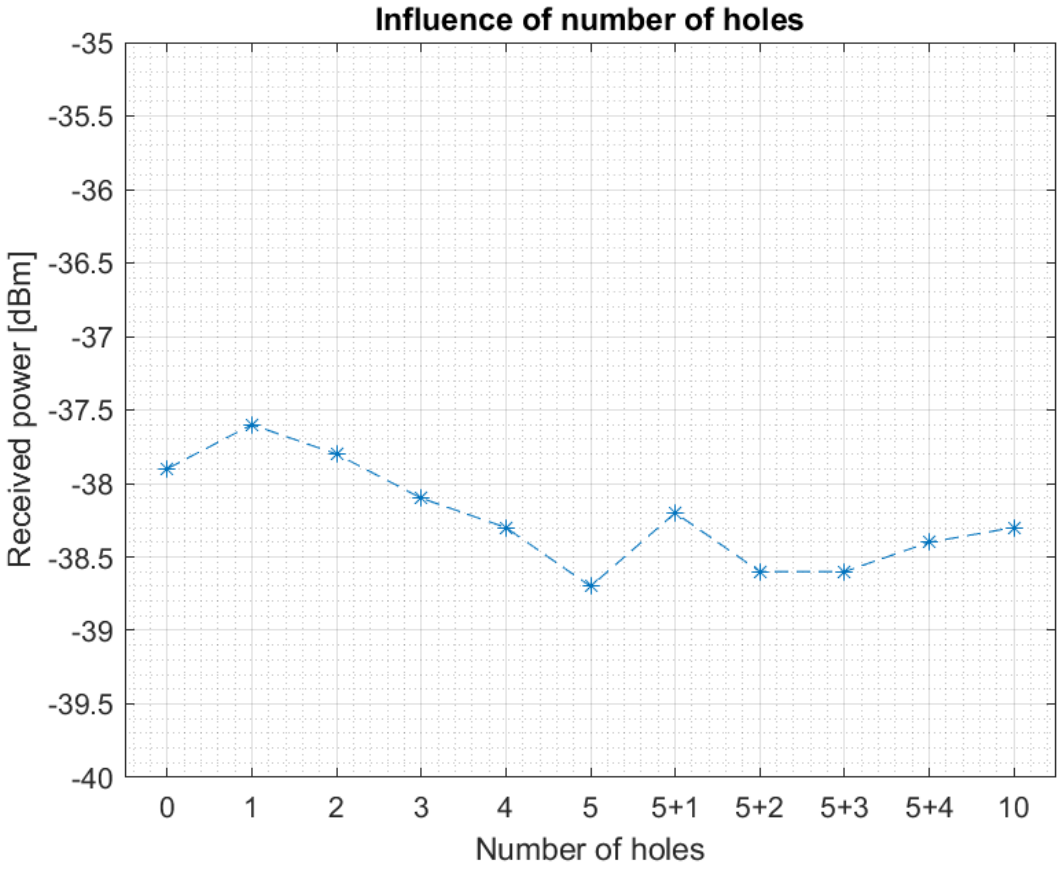

Figure 29: Influence of the number of holes

Once again, the variability of the measurements remains small. As the relative difference between the highest and lowest received power now equals 2.93%, one can again not conclude that the number of holes has a significant influence on the received power.

In general, both the influence of the position and the number of holes was found negligible for this setup. This is logical since a Two-Ray model is mostly used for tall antenna towers (taller than 50 m) that are separated by several kilometers. This could not be further from the setup used in this report. From a mathematical point of view, during the development of the equation of the Two-Ray model, several assumptions are made. For instance, one assumes that the distance between the two antennas is large with respect to the height of both antennas. Or, quantitatively:

$$d > \frac{20\pi h_t h_r}{3\lambda} \approx \frac{20 h_t h_r}{\lambda} \tag{11}$$

When calculating the right hand side for an antenna height of 1.5 m, the minimal distance for the criterion to be met corresponds to 174.17 m. Therefore, the Two-Ray model cannot be used to described the setup used in this report.

4.3 Small-scale fading

Finally, the characteristics of a small-scale flat fading channel will be determined. Small-scale fading refers to rapid fluctuations or distortions of the signal power over a brief time period. In order to simulate this, the two antennas were placed at each end of the laboratory, one as a transmitter, the other as a receiver. Measurements of the peak power at reception side were logged every 100ms for a total of 1000 iterations. During this period, deliberate distortions were introduced on the channel by moving metal objects and people between the two antennas, simulating a realistic traffic environment with real-life distortions such as passing cars or motorcycles. The measured data is plotted in Figure 30.

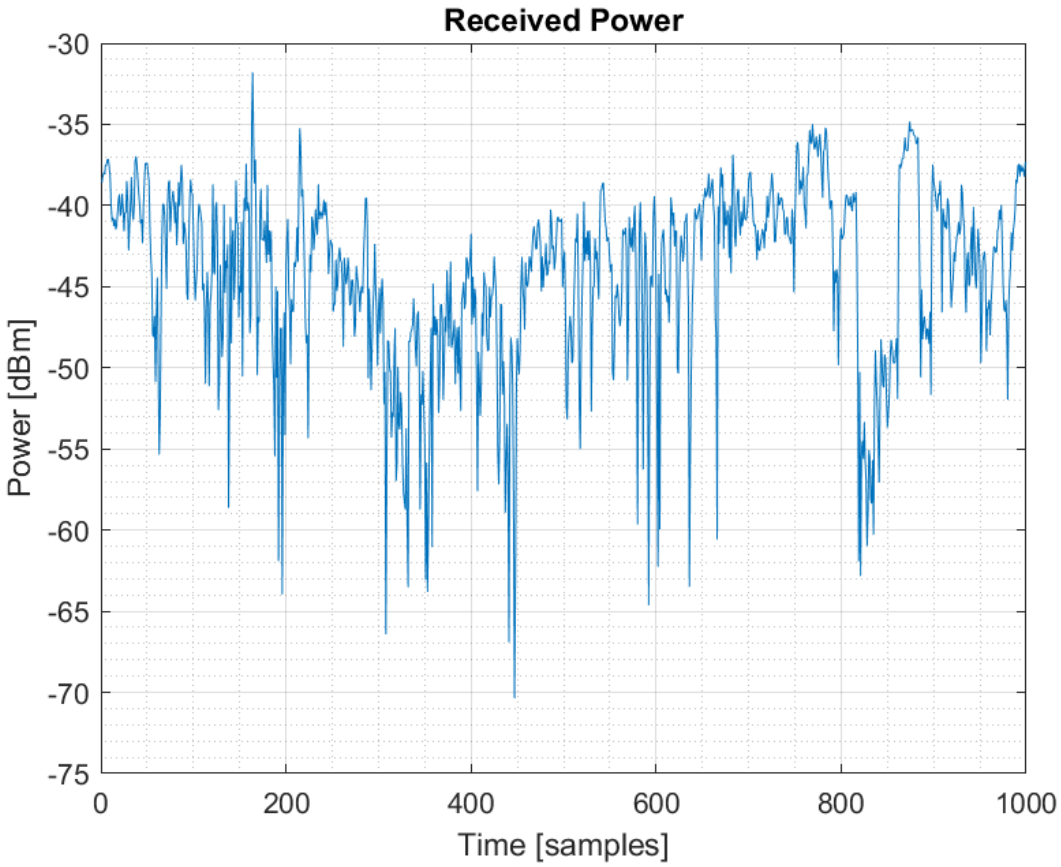

Figure 30: Received data

One clearly notices some outliers, both in terms of maximum and minimum values. The negative peaks are sometimes referred to as *deep fades*. These peaks are indications of a very poor transmission channel between the two antennas.

In general, the data seems random in nature. However, a model exists to approach small-scale fading. Since there is a direct Line-of-Sight (LOS) between the two antennas, a clear dominant signal component is present, leading to a Rician envelope distribution [5]. This Rician distribution is derived from a Rayleigh distribution but adapted to incorporate the direct contribution of the LOS. It is characterized by the following probability density function (pdf):

$$\text{pdf}(x) = \frac{x}{\sigma^2} \exp\left(\frac{-(x^2+s^2)}{2\sigma^2}\right) I_0\left(\frac{xs}{\sigma^2}\right) \tag{12}$$

with:

1. s: the non-centrality parameter
2. σ: the scale parameter
3. I_0: the modified Bessel function of the first kind with order 0

It is common practice to completely characterize a Rician distribution using the so-called *shape parameter* K, defined as follows:

$$K = 10 \log_{10}\left(\frac{s^2}{2\sigma^2}\right) \tag{13}$$

Because Figure 30 does not easily allow to draw conclusions, a histogram of the data is represented. Furthermore, a Rician distribution is fitted on the data to allow statistical analysis. Both are shown in the following Figure. Note that the histogram was normalized.

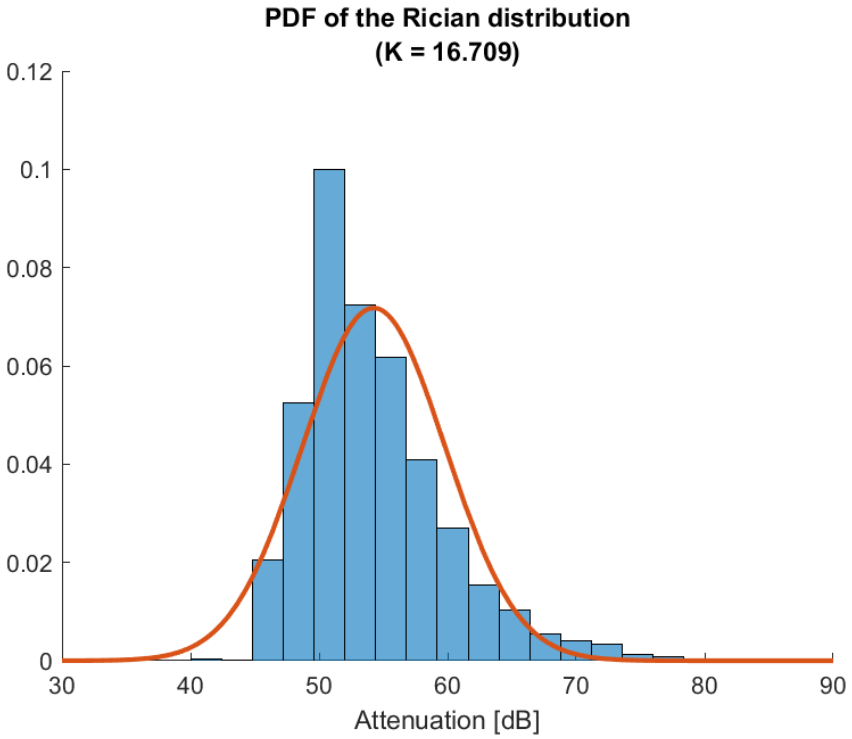

Figure 31: Rician distribution

One can immediately see that the histogram corresponds well to the pdf. This hints that the fitted distribution is coherent to the data. Only around 50 dB, there is an outlier. The correspondence will never be perfect of course.

The fitted pdf is centered around 53.96 dB and has a standard deviation of 5.57 dB. A confidence interval is also calculated: there is a 95.48% chance that the attenuation lies between 42.82 dB and 65.11 dB. This allows to entirely characterize the small-scale fading for the given scenario.

5 Conclusion

In this report, we have characterised two handcrafted antennas. After a short description of the provided equipment, we discussed the measurements of the reflection coefficient and the Voltage Standing Wave Ratio. Afterwards, the center frequency and the corresponding working bandwidth were determined. For both antennas, the center frequency was chosen at $f = 1.16\ GHz$, despite a small deviation for one of the two antennas. Next, the three regions around the antenna were modelled. For both antennas, the boundaries of the Fresnel and Fraunhofer regions coincide at a distance of 3.38 m.

Before continuing with the determination of the different radiation patterns, we verified whether the antennas were correctly matched. From our calculations, we found that short-circuited stubs of respectively 0.24 cm and 0.57 cm were required to properly match antenna A and B to the impedance of the line. For practical reasons, these shorted stubs were not actually implemented. Then, we concluded the radiation pattern both in azimuth and elevation corresponded to the theoretical versions. The final step of the characterization was to determine the antenna gain. For both antennas, a negative value for the gain was found. Given these antennas are handcrafted, this is not too surprising.

The second part in the analysis of the antennas consisted in discussing several propagation models. First of all, the free space link model is discussed. We showed that the received power is indeed proportional to the distance from the transmitting antenna according to an inverse square law. Secondly, the influence of a polarization mismatch and a relative angle between the two antennas is analyzed. It is shown that no mismatch leads to maximum received power. The second model we analyzed is the Two-Ray model. It is shown that nor the number of so-called holes, nor their position has a significant influence on the received power level. Given the assumptions under which the Two-Ray model was constructed, this is only logical. The last part of this report covers the small-scale fading channel. A real-life environment was simulated by moving metal objects and people between the two antennas. Finally, the parameters of the Rician distribution were determined to completely characterize the small-scale fading.

References

[1] Iacopo Giangrandi. Sept. 2000. URL: https://www.giangrandi.org/electronics/anttool/regions.shtml?fbclid=IwAR37w-NLVzRIYwabmaApN1H28ka2BOGewiNUTOKyhhSYm0Bkr3yDsW-TP7w.

[2] Anitha Govind. *Antenna Impedance Matching – Simplified.*

[3] *RG58 coaxial cable - farnell.* July 2022. URL: https://www.farnell.com/datasheets/2095749.pdf.

[4] *Gain (antenna).* Dec. 2022. URL: https://en.wikipedia.org/wiki/Gain_(antenna).

[5] *Rice distribution.* Nov. 2022. URL: https://en.wikipedia.org/wiki/Rice_distribution.

[6] *What are Near Field and Far Field Regions of an Antenna?* May 2018. URL: https://www.everythingrf.com/community/what-are-near-field-and-far-field-regions-of-an-antenna.

[7] *Two-ray ground-reflection model.* Feb. 2022. URL: https://en.wikipedia.org/wiki/Two-ray_ground-reflection_model.

[8] Sept. 2016. URL: https://help.agi.com/stk/11.0.1/Content/comm/tworay.htm.